

Supplementary Materials

Albumin-Gold Nanorod Nanoplatform for Cell-Mediated Tumortropic Delivery with Homogenous ChemoDrug Distribution and Enhanced Retention Ability

Hsien-Ting Chiu, Cheng-Kuan Su, Yuh-Chang Sun, Chi-Shiun Chiang and Yu-Fen Huang*

Corresponding Author

Prof. Yu-Fen Huang

Department of Biomedical Engineering and Environmental Sciences, National Tsing Hua University, Hsinchu

30013, Taiwan, ROC

yufen@mx.nthu.edu.tw

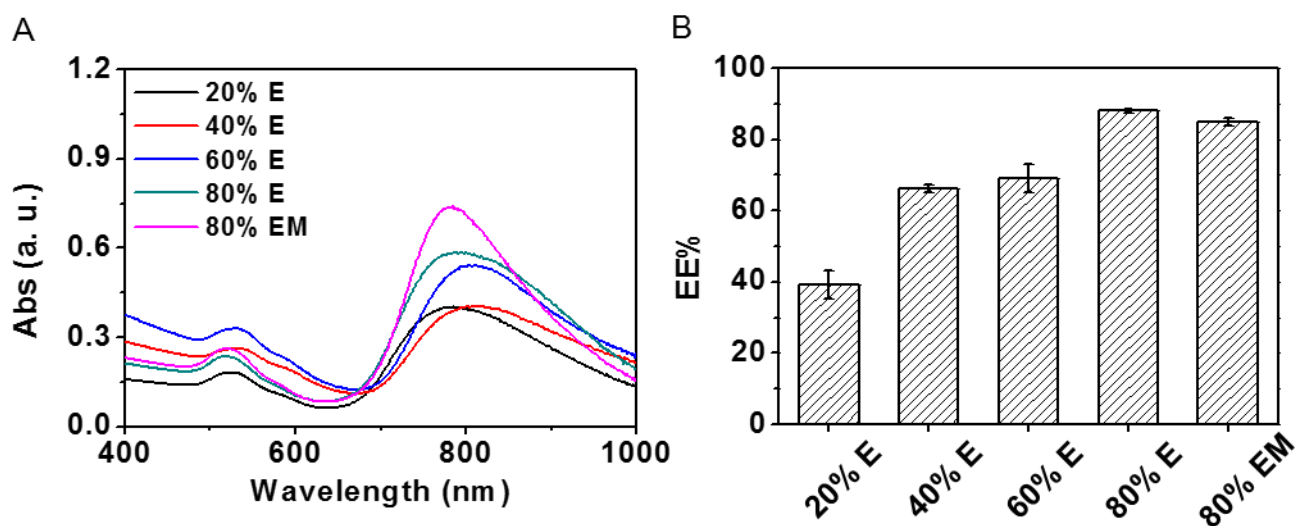


Figure S1. Investigation the desolvation effect of organic solvents on NR@SAs fabrication. SA solution (3 μ M) was added into an Au NRs suspension (2 \times , 0.6 nM), followed by 12 h incubation with 20–80% ethanol or 80% EM (40% ethanol + 40% methanol) solution, respectively. After the organic solvent was removed by centrifugation and the sample was re-dispersed in DI water, the (A) UV–Vis spectra of the resultant nanoconjugates were obtained. (B) The loading capacity of SA onto Au NRs was evaluated under different desolvation conditions. TRITC-labeled SA was used for quantitative fluorescence analysis (excitation/emission: 540/572 nm).

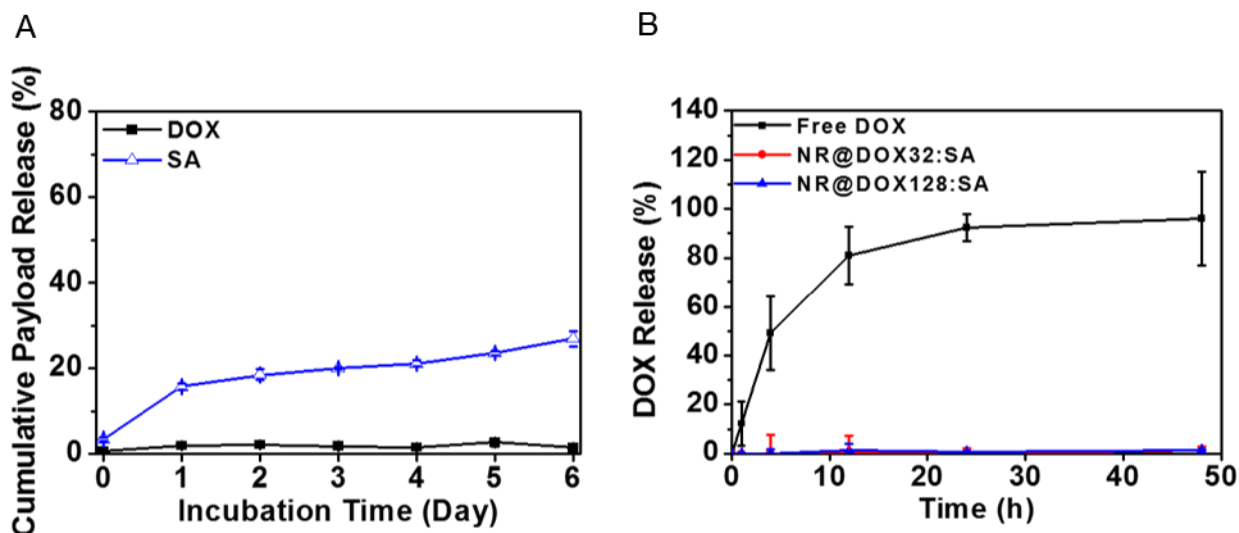


Figure S2. The profile of payload release from pristine nanoparticles. (A) 2.4 nM NR@DOX32:SA or NR@SA-TRITC were immersed in PBS (150 μ L) and the supernatants were collected at each time point by centrifugation (3500 rpm, 10 min). DOX and SA-TRITC fluorescence was measured using a plate reader. (B) The release kinetics of drug molecules from pristine nanoparticles was further by means of a dynamic dialysis technique. 500 μ L of NR@DOX32:SAs, NR@DOX128:SAs and free DOX (47.6 μ M) was added into a 3.5K MWCO dialysis devices (Slide-A-Lyzer MINI Dialysis Devices, Thermal Fisher) and placed in a microcentrifuge tube that is filled with PBS (1 mL). A stir bar was used for continuous stirring (500 rpm). The fluorescence signal of drug molecules released into dialysis buffer was measured at each time point during dialysis.

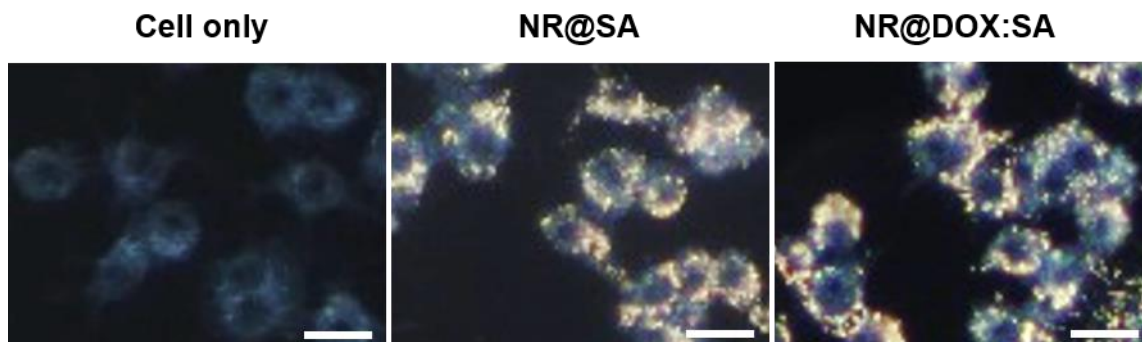


Figure S3. Dark-field images of macrophages (RAW 264.7) incubated for 2 h with NR@SAs and NR@DOX:SAs. The Au NRs concentration of all samples was maintained at 2.4 nM. Treated cells were recovered upon 6 h to conduct microscopic examination. Scale bar: 20 μm .

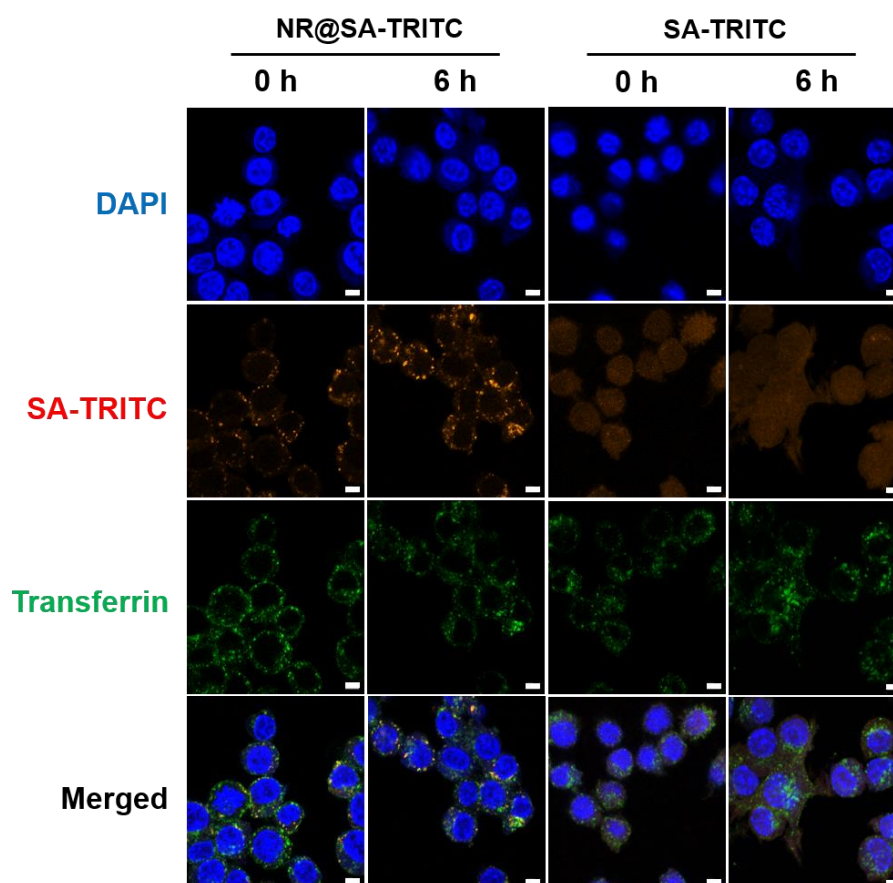


Figure S4. The intracellular transport of fluorescently labeled SA within macrophages incubated with NR@SA-TRITC and SA-TRITC. The Au NRs concentration of all samples was maintained at 2.4 nM. Treated cells were visualized at different recovery time points by laser scanning confocal microscopy. Nuclei were stained with DAPI in blue, and the acidic endolysosomal compartments were stained with transferrin-Alexa 633 in green. Scale bar: 5 μ m.

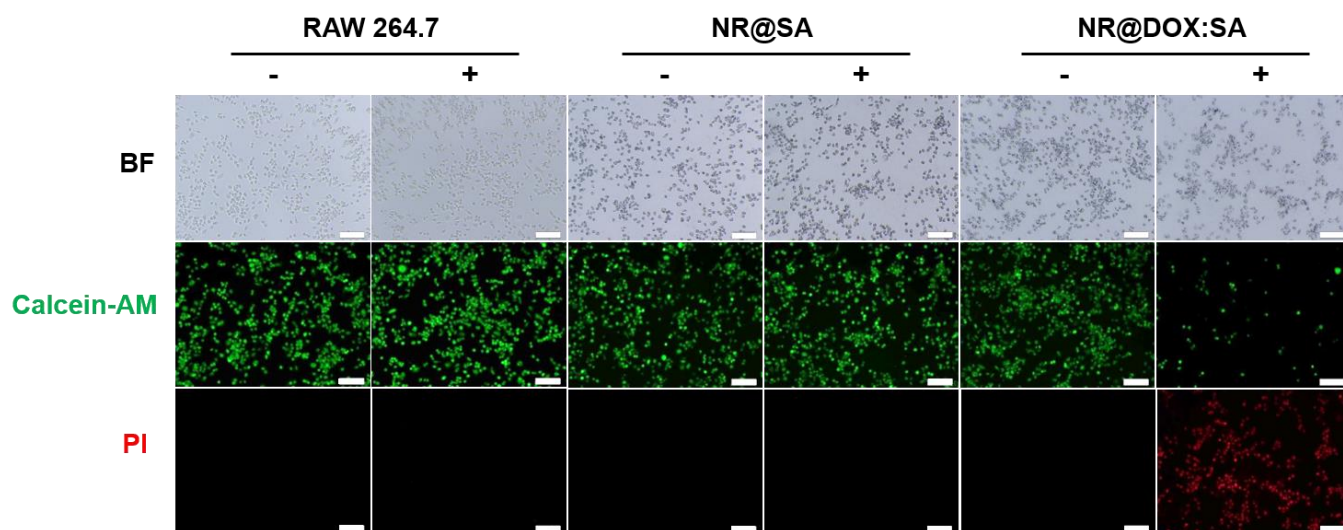


Figure S5. Live/dead cell double staining assay of macrophages (RAW 264.7) treated with different nanoagents followed by NIR irradiation (808 nm, 2.65W/cm², 1 h). Cells were stained with 1.5 μM calcein-AM (green) and 2.5 μM propidium iodide (PI, red) for 30 min before observation by fluorescence microscopy. Scale bars are 100 μm.

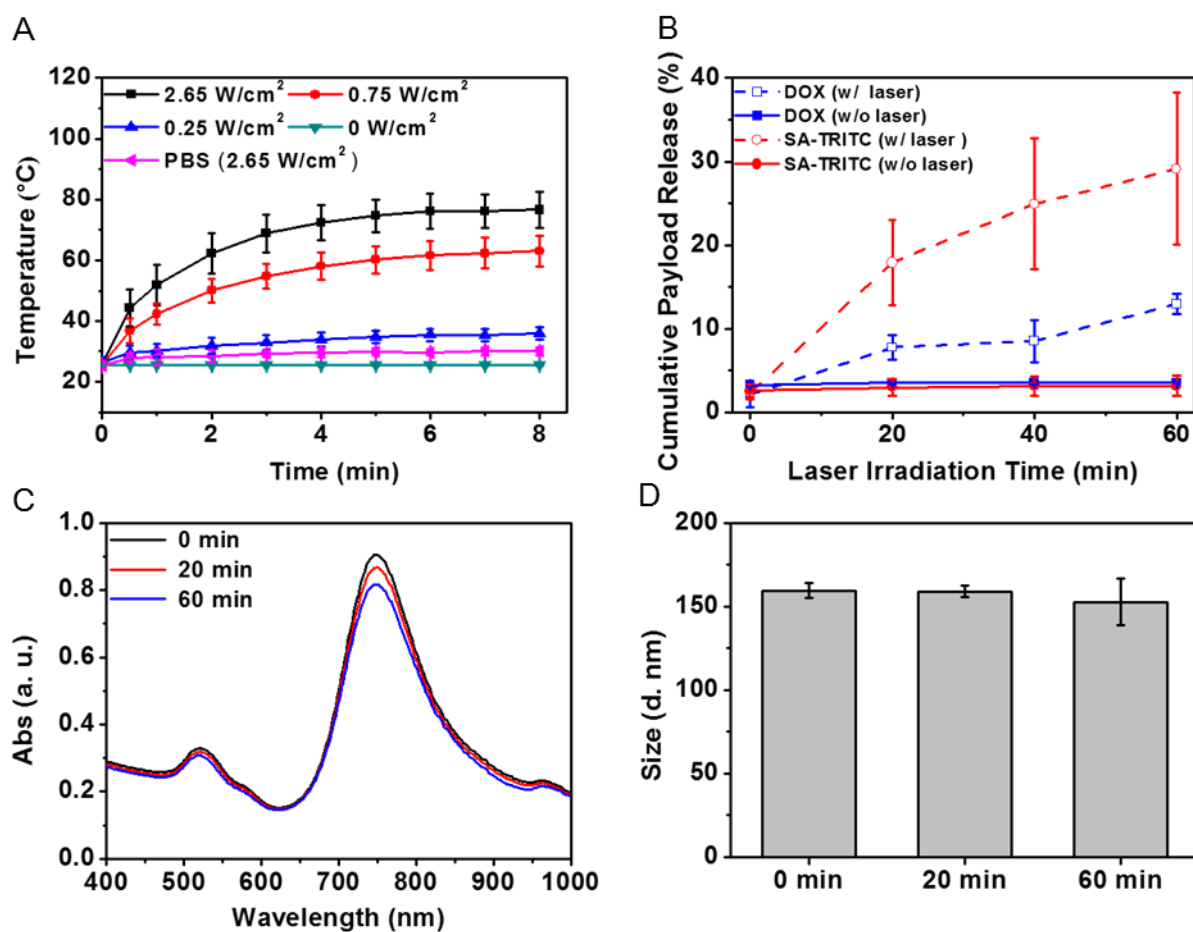


Figure S6. (A) Temperature increase of 0.6 nM NR@DOX:SAs or PBS under NIR laser irradiation at different laser power densities. (B) DOX and SA-TRITC release study of NR@DOX:SAs and NR@SAs under NIR light irradiation (808 nm, 2.65 W/cm²) over time in PBS. (C) UV-Vis spectra and (D) hydrodynamic size of NR@DOX:SAs was measured at 20 min time intervals for 1 h under NIR light exposure.

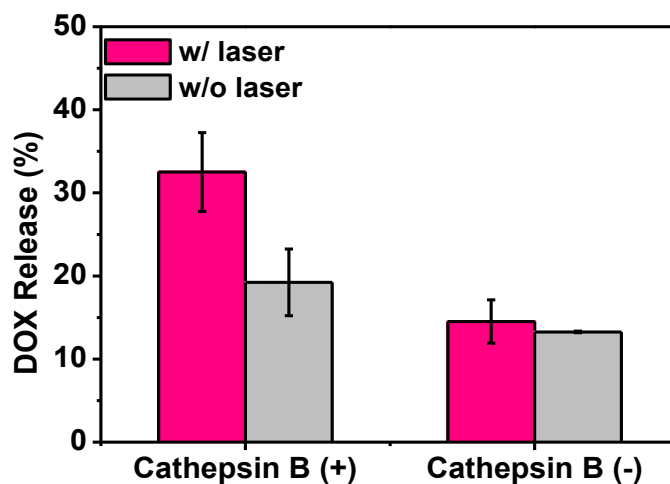


Figure S7. NIR light-mediated DOX release was further improved for NR@DOX:SAs pre-treated with cathepsin B, a lysosomal cysteine protease. 1.6 U/ mL of cathepsin B was immersed in activation buffer (20 mM 1,4-dithiothreitol and 10 mM ethylenediaminetetraacetic acid) for 15 min at 37.5°C. As-prepared NR@DOX:SAs (2.4 nM) was first incubated with pre-activated 0.1 U/mL cathepsin B in lysosomal buffer (60 mM citric acid, 140 mM dibasic sodium phosphate and 23.5 mg/mL L-cysteine) containing 0.6% SA for 2 h. Then, nanoparticles were diluted with lysosomal buffer to 0.6 nM and exposed to 2.65 W/cm² NIR laser for 1 h. The fluorescence of DOX was measured by plate reader to determine the amount of released DOX.

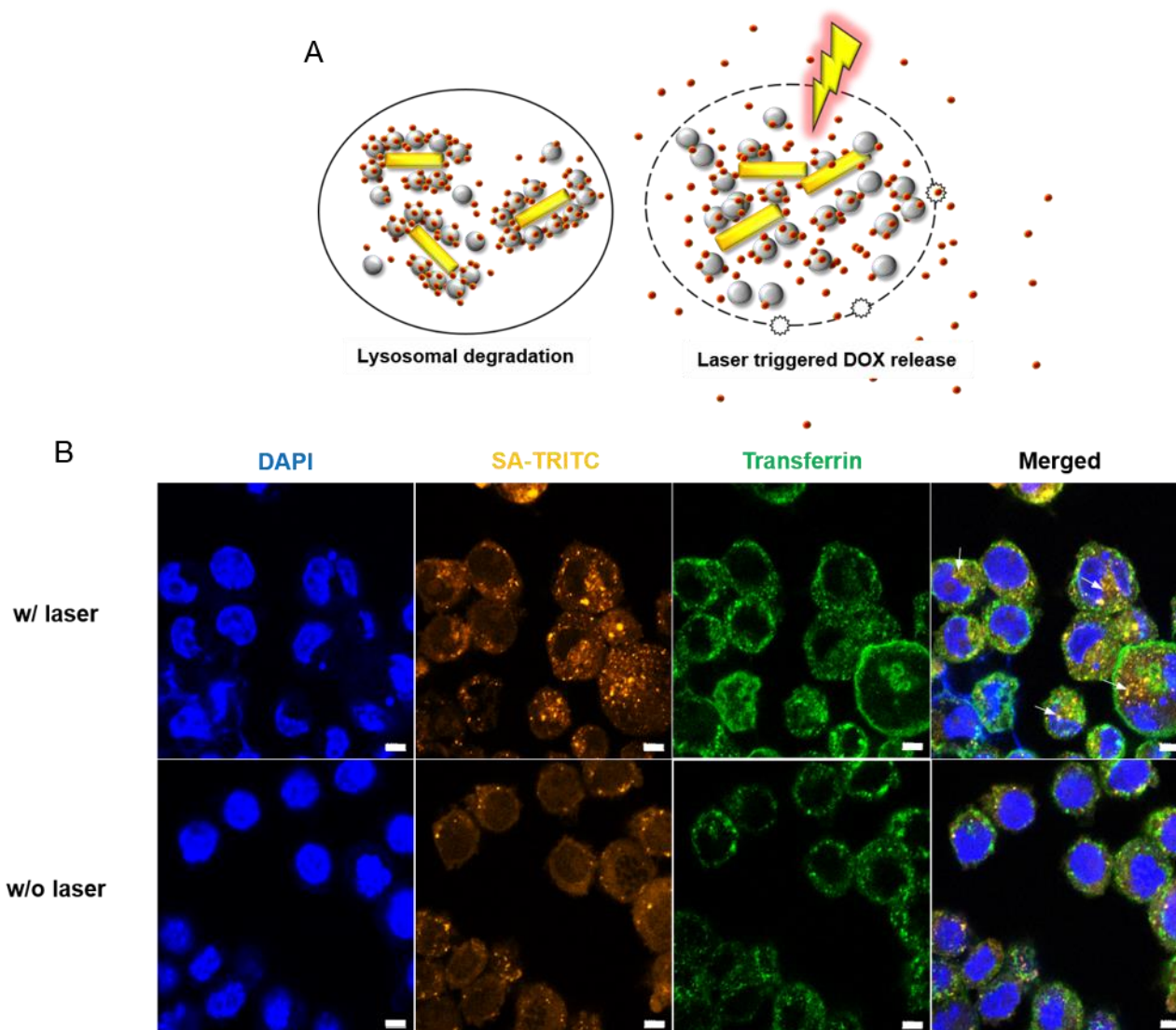


Figure S8. (a) Schematic of NR@DOX:SA-laden macrophages in response to NIR activation. (b) Effect of NIR irradiation on intracellular SA-TRITC transport was visualized in NR@DOX:SA-treated macrophages (RAW 264.7) by laser scanning confocal microscopy. Nuclei were stained with DAPI (1 μ M, 15 min) in blue and the acidic endolysosomal compartments were stained with transferrin-Alexa 633 (300 nM, 30 min) in green. The

white arrows indicate that the location where SA fluorescence was not overlapped with the endo-lysosomal marker. Scale bar: 5 μm .

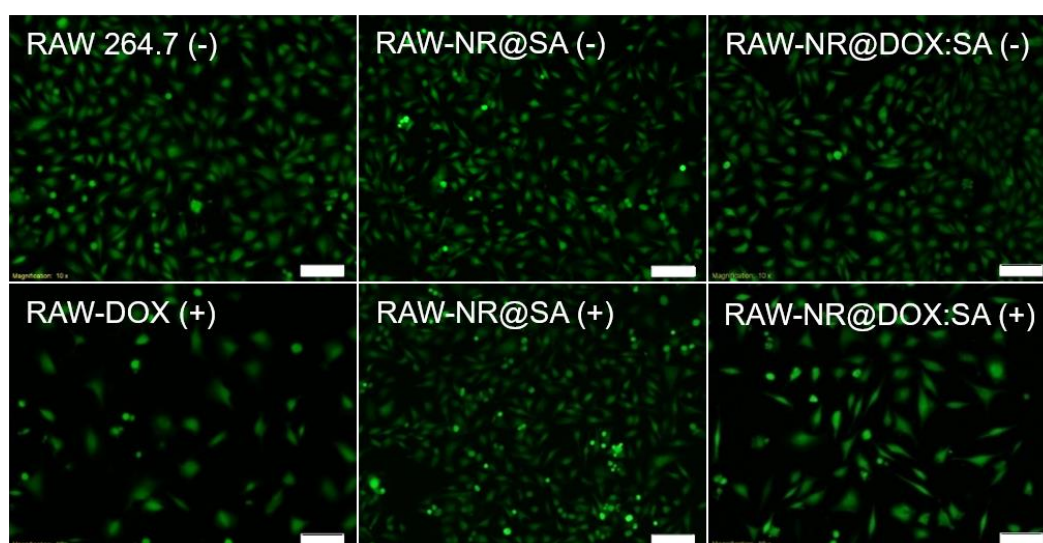


Figure S9. Monitoring of cell number of Tramp-C1 cells in response to CM taken from macrophages under different treatment. Tramp-C1 cells were stained with 1.5 μM calcein-AM (green) for 30 min before fluorescence microscopy observation. Scale bars are 100 μm .

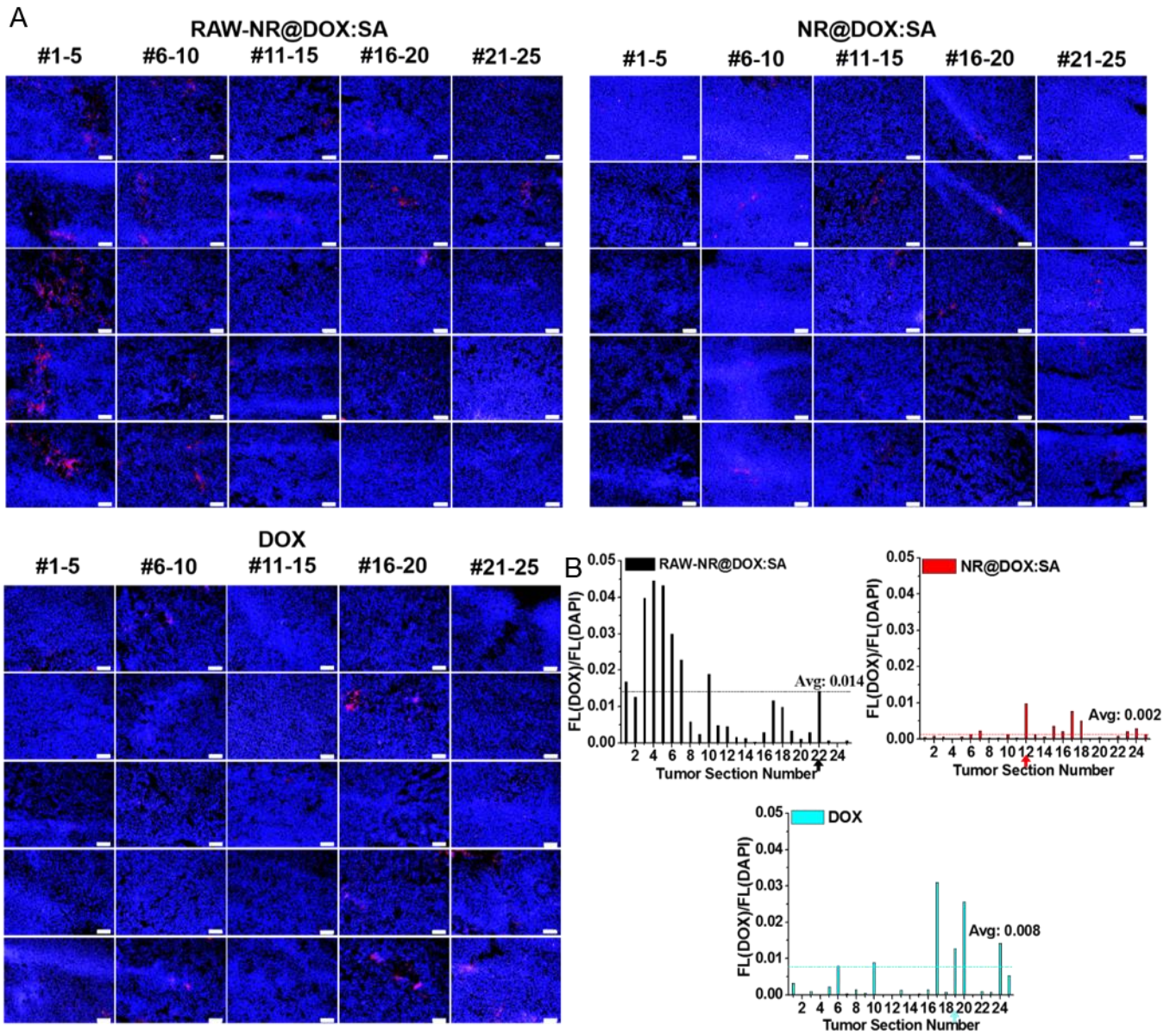


Figure S10. The evaluation of chemodrug retention and distribution. On day 11, intratumoral drug distribution of the tumor harvested from mice injected intratumorally with RAW-NR@SAs, NR@SAs, and DOX. (A) DOX fluorescence images and (B) quantitative analysis of images from 25 z-sections of the corresponding tumor at 550- μ m intervals were investigated. The total fluorescence intensity of DOX and DAPI in the corresponding area ($5 \times 5 \text{ mm}^2$, yellow dashed rectangle) of each section was quantified using the Image J software and is presented as the DOX/DAPI signal ratio. The largest tumor cross section of each treatment group was marked as #22, #12, and #19, respectively. Scale bar: 100 μ m.

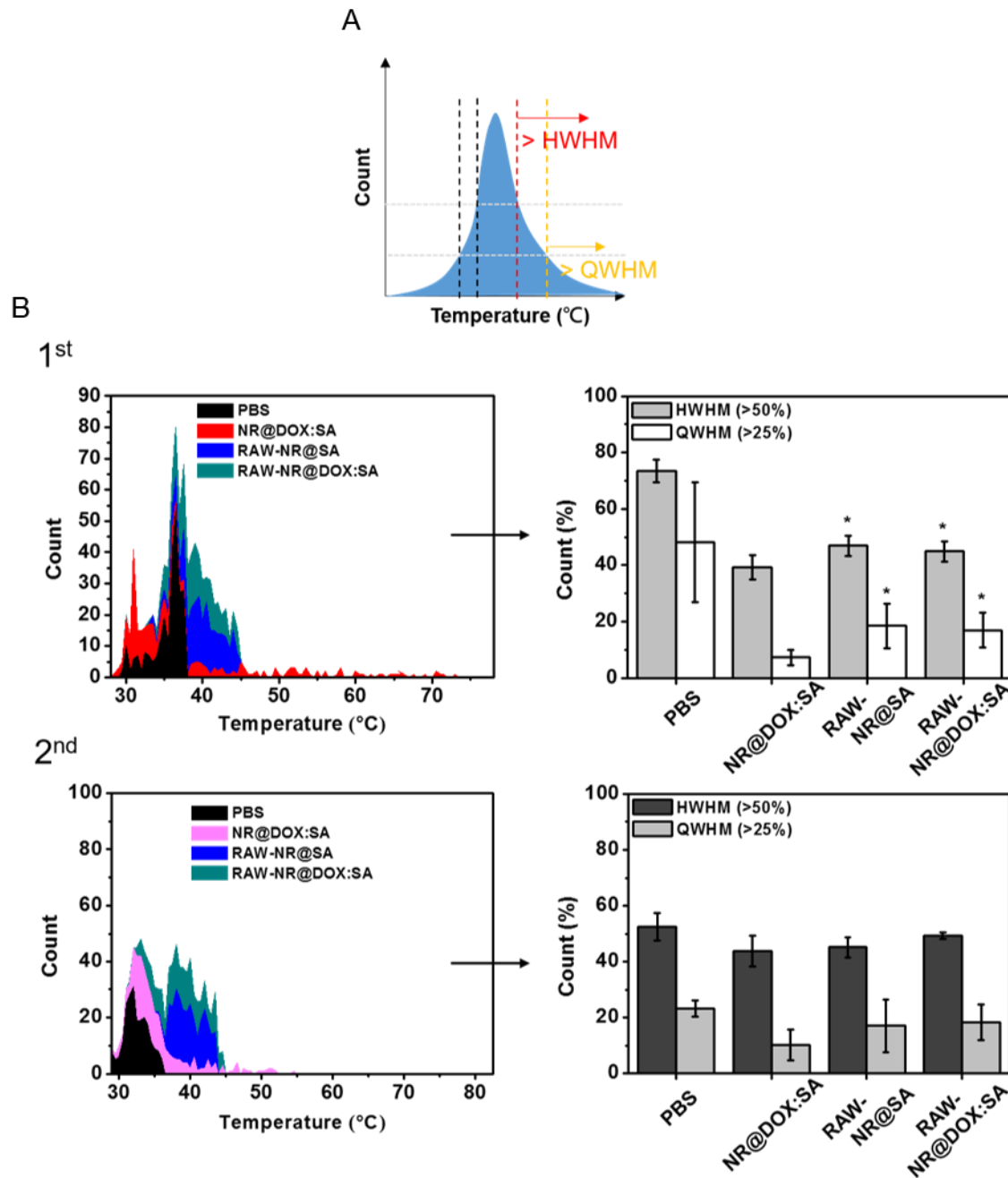
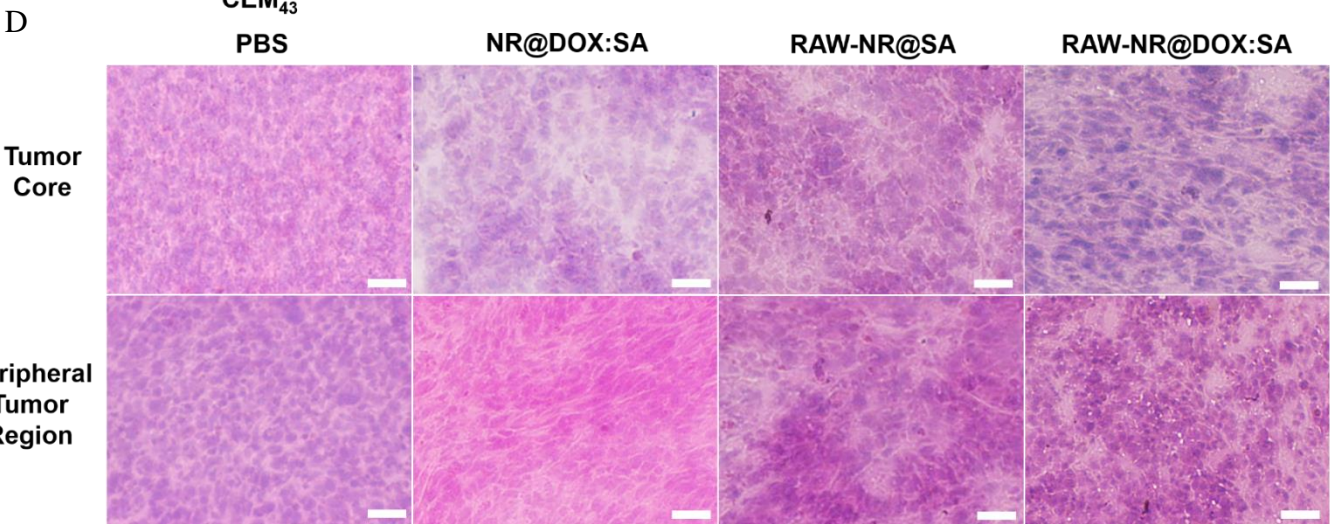
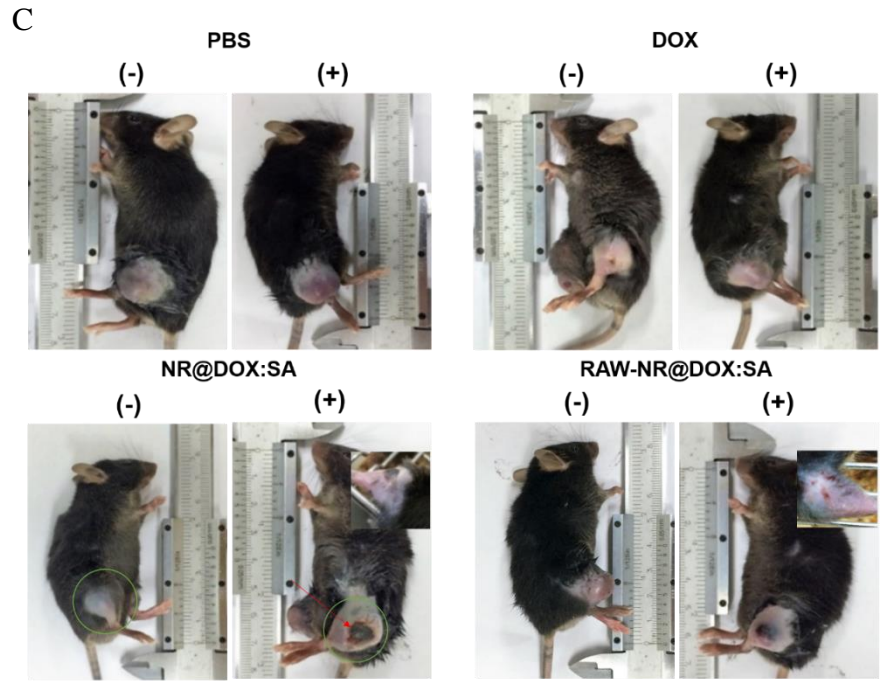
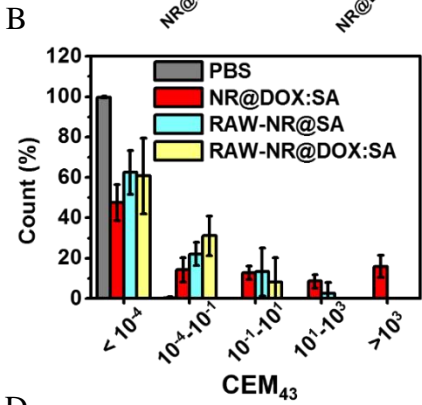
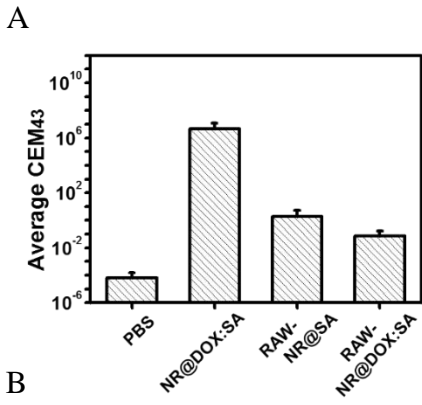
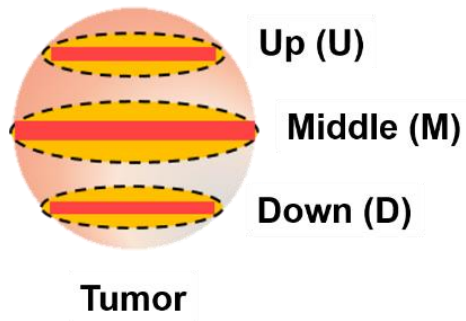


Figure S11. Statistical analysis of thermal distribution. (A) Schematic illustration for the half and quarter width at half maximum (HWHM and QWHM) analysis. (B) Each thermal profile was obtained from PBS, NR@DOX:SAs, RAW-NR@SAs and RAW-NR@DOX:SAs treated mice after the first and second time NIR laser irradiation (808 nm, 0.75 W/cm², 3 min). Every detected count within laser spot from each group was through HWHM and QWHM analysis ($n = 3-5$, $*p < 0.05$ versus NR@DOX:SAs treated mice).



E



F

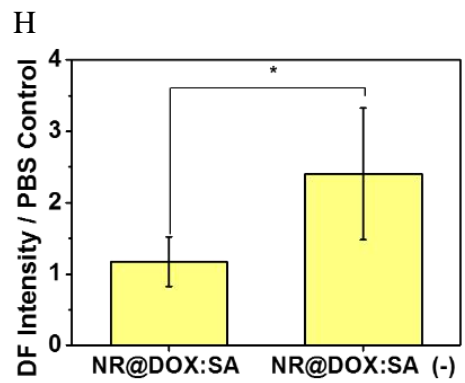
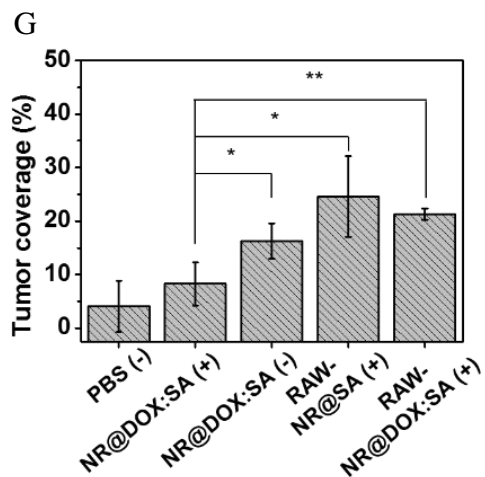
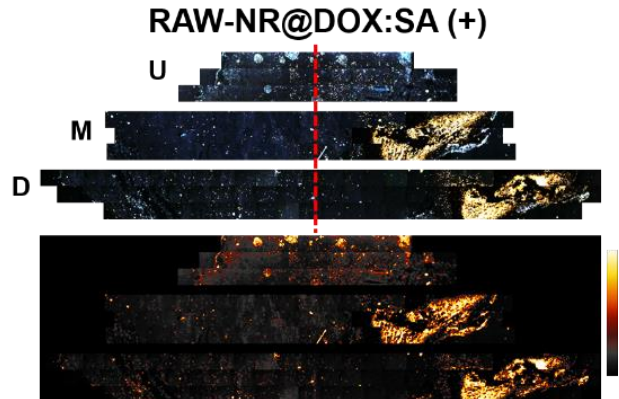
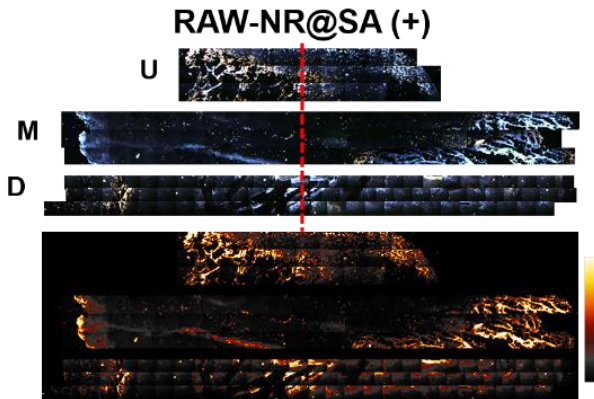
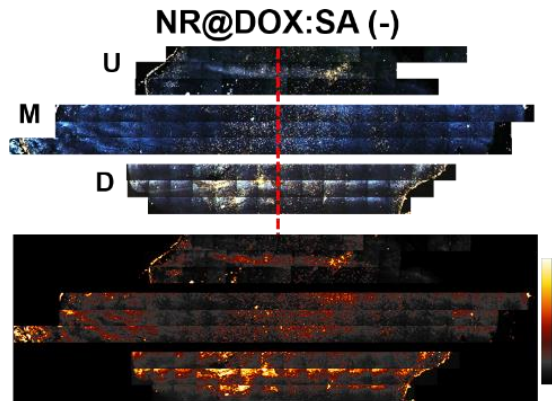
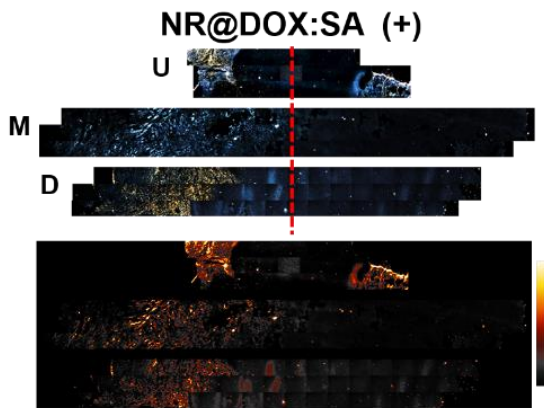
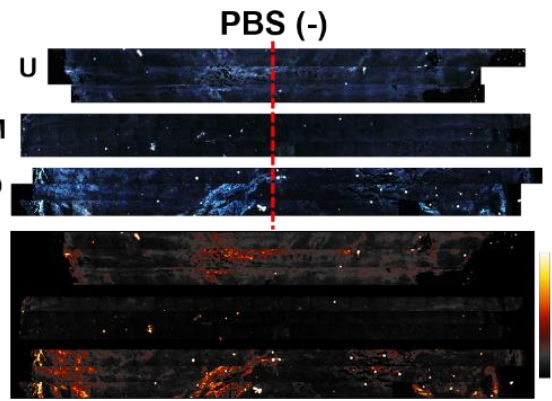


Figure S12. *In vivo* investigations of the photothermal damage and resultant biological effects. Each detected count within the laser spot monitored by IR camera on day 1 after the first NIR laser irradiation treatment was converted to CEM₄₃. The (A) average and (B) corresponding distribution of CEM₄₃ were first obtained. Subsequently, on day 4, (C) digital images of the tumor-bearing mice (who received therapeutic drug injections two times and NIR laser irradiation one time) were recorded before sacrifice. Red arrow indicates bleeding from the unhealed wound. Green circle highlights the tumor color in the pristine NR@DOX:SA group after second injection with or without first NIR laser irradiation. Inset: NR@DOX:SA- or RAW-NR@DOX:SA (+)-treated mice at 12 h post-NIR laser treatment. The harvested tumor was analyzed through (D) H&E staining of the central or peripheral tumor region. Scale bar: 50 μ m. Furthermore, several tumor sections as described in (E) were obtained for dark-field microscopic observations. (F) The recorded dark-field images from each tissue slide were combined and preprocessed using the Image J software program to flatten the light fluctuations. On the basis of the triple standard difference methods, a signal detecting over 3-fold σ of the average signal from the PBS control group was defined as the threshold. Signals beyond the threshold were further calculated to obtain the (G) tumor coverage and (H) corresponding average intensity ratio (NR@DOX:SA (+/-) divided by the PBS control group). The area of the signals beyond the defined threshold divided by the total area of the tumor section was defined as tumor coverage; the average intensity of scattering light was calculated by the average number of pixels from each count ($n = 3$, * $p < 0.05$ or ** $p < 0.01$).

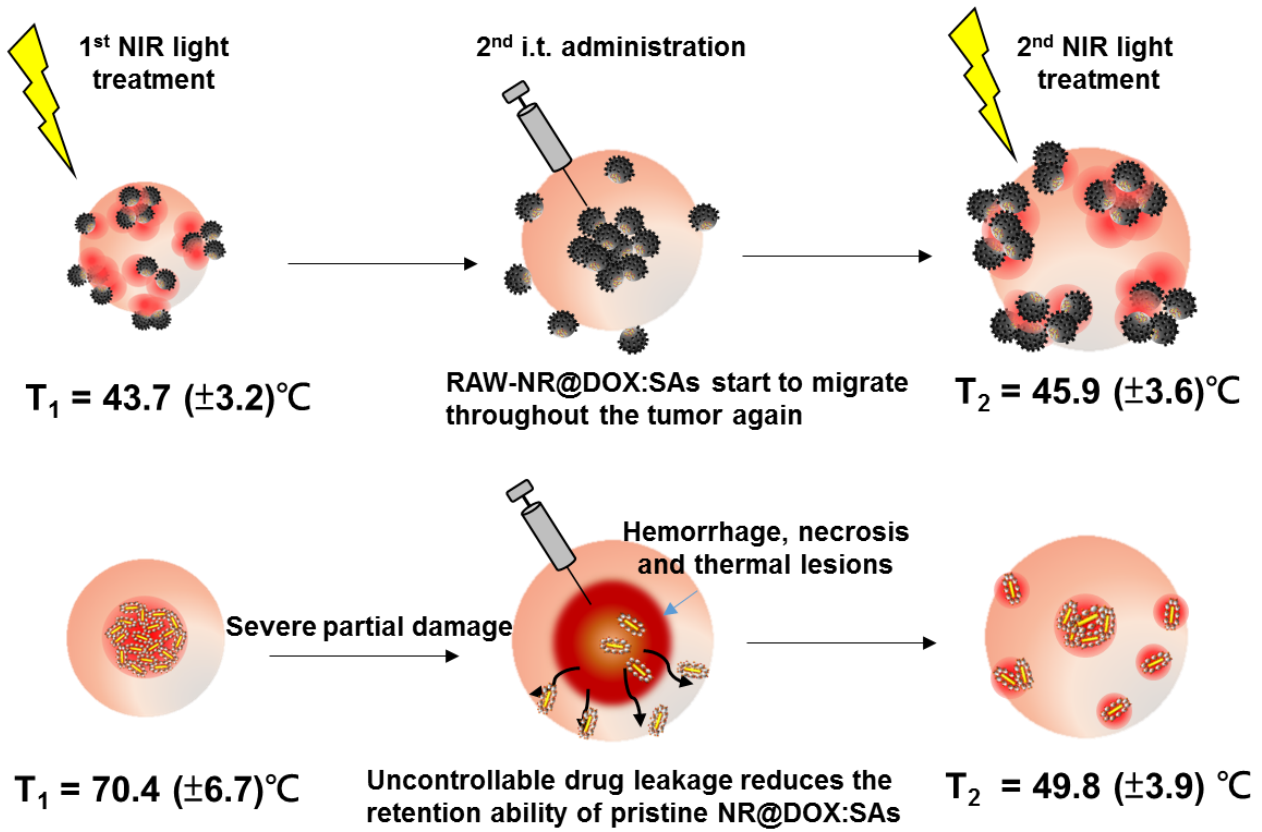


Figure S13. Schematic illustration of the mechanism why the increased temperature from the second time NIR laser treatment of pristine NR@DOX:SAs treated mice compared to that of the first time treatment was largely decreased.

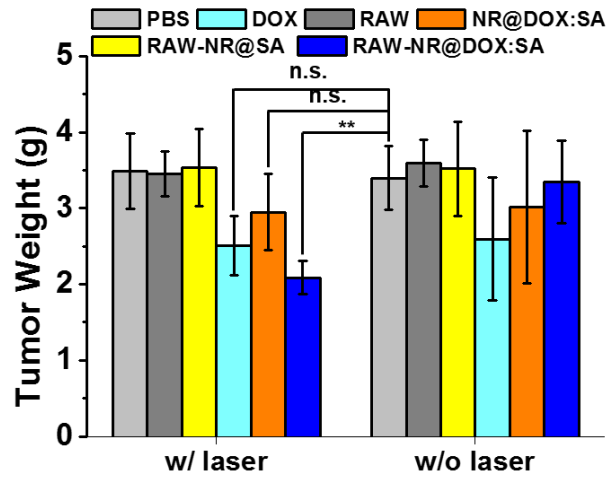


Figure S14. Xenograft tumors of mice receiving various treatments were harvested and weighed on day 11. ($n = 4-5$, $**p < 0.01$, or n.s. > 0.05 .)

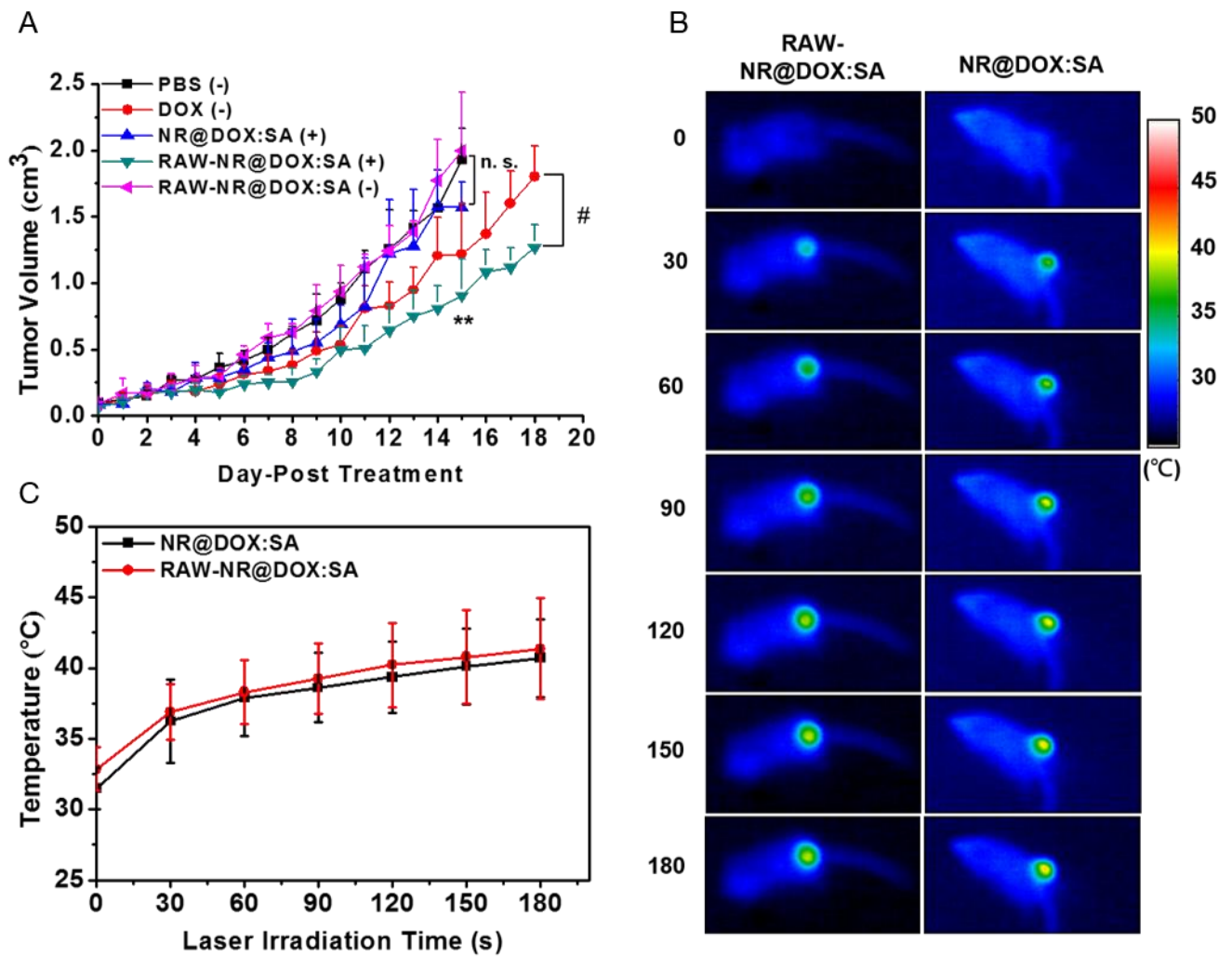


Figure S15. *In vivo* photothermal effect by intravenous injection of NR@DOX:SAs or RAW-NR@DOX:SAs. (A) Relative tumor growth curves of Tramp-C1 tumor-bearing mice received different therapeutic treatments intravenously. $n = 6$, $**p < 0.01$ or n.s. > 0.05 versus PBS-treated control. # $p < 0.05$ versus DOX (-). (B) Thermal image and (C) the corresponding rising temperature of treated mice under 808 nm light irradiation (0.75 W/cm², 3 min) at 24 h post-injection.